Electronic Supplementary Material (ESI) for Journal of Materials Chemistry B.

Electronic Supplementary Information

Nanovoid formation induces property variation within and across individual silkworm silk threads

Hamish C. Craig[a], Yin Yao[b], Nicholas Ariotti[b], Mohan Setty[c], Rechana Ramadevi[c], Michael M. Kasumovic[a], Rangam Rajkhowa[c], Aditya Rawal[d]*, and Sean J. Blamires[a,d]*

[a]*School of Biological, Earth and Environmental Science, UNSW Sydney, 2052, Australia.*

[b]*Electron Microscopy Unit, Mark Wainwright Analytical Centre, UNSW Sydney, 2052, Australia.*

[c]*Institute for Frontier Materials, Deakin University, Geelong, 3216, Australia.*

[d]*Nuclear Magnetic Resonance Facility, Mark Wainwright Analytical Centre, UNSW Sydney, 2052, Australia.*

Supplementary Figures

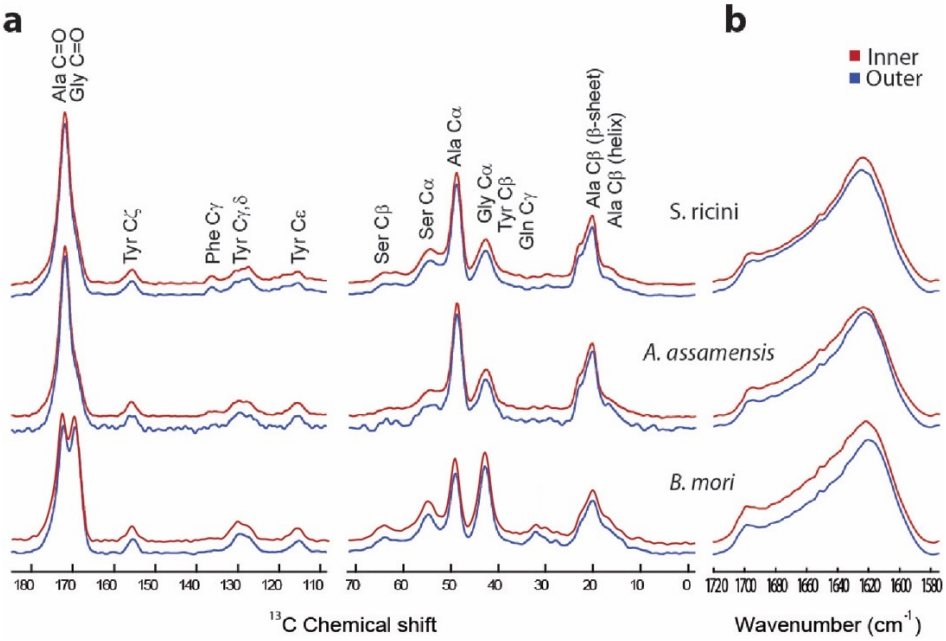

Fig. S1a. 1D -C CPMAS NMR spectra showing transposable nature of inner and outer sections for Mulberry (*B. mori*) silk, Muga (*A. assamensis*) silk and Eril (*S. c. ricini*) silk, highlighting the chemical homogeneity in amino acids structure throughout the fiber. **b.** FTIR spectra showing Amide I peak demonstrating the homogeneity of secondary structure between the inner and outer sections of the silk fibers within each species.

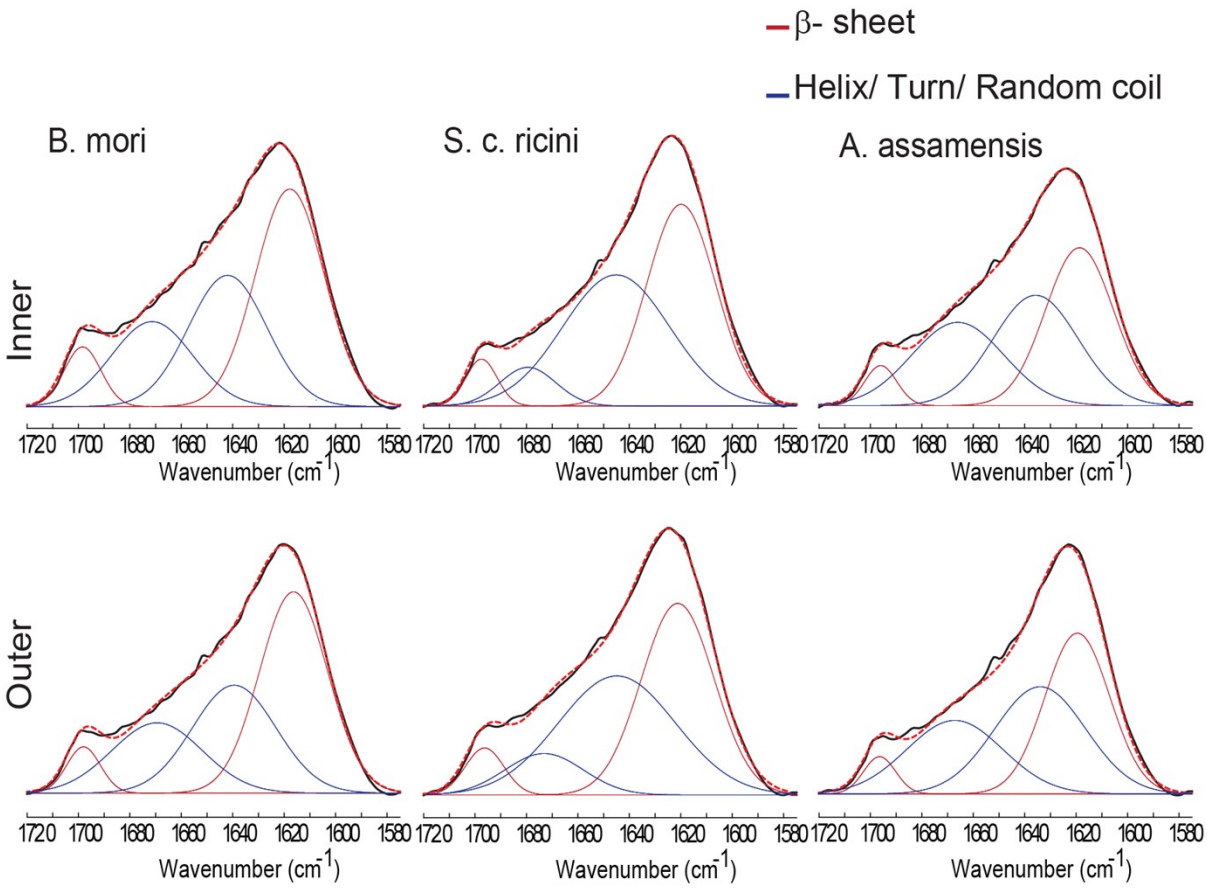

Fig. S2. Expanded FTIR spectra showing Amide I peak demonstrating along with the peak deconvolution for the b-sheet and helix/turn/random coil fractions in the silk fibroin structure for the silk from the inner and outer cocoon section from Mulberry (*B. mori*) silk, Eri (*S. c. ricini*) silk and Muga (*A. assamensis*) silk.

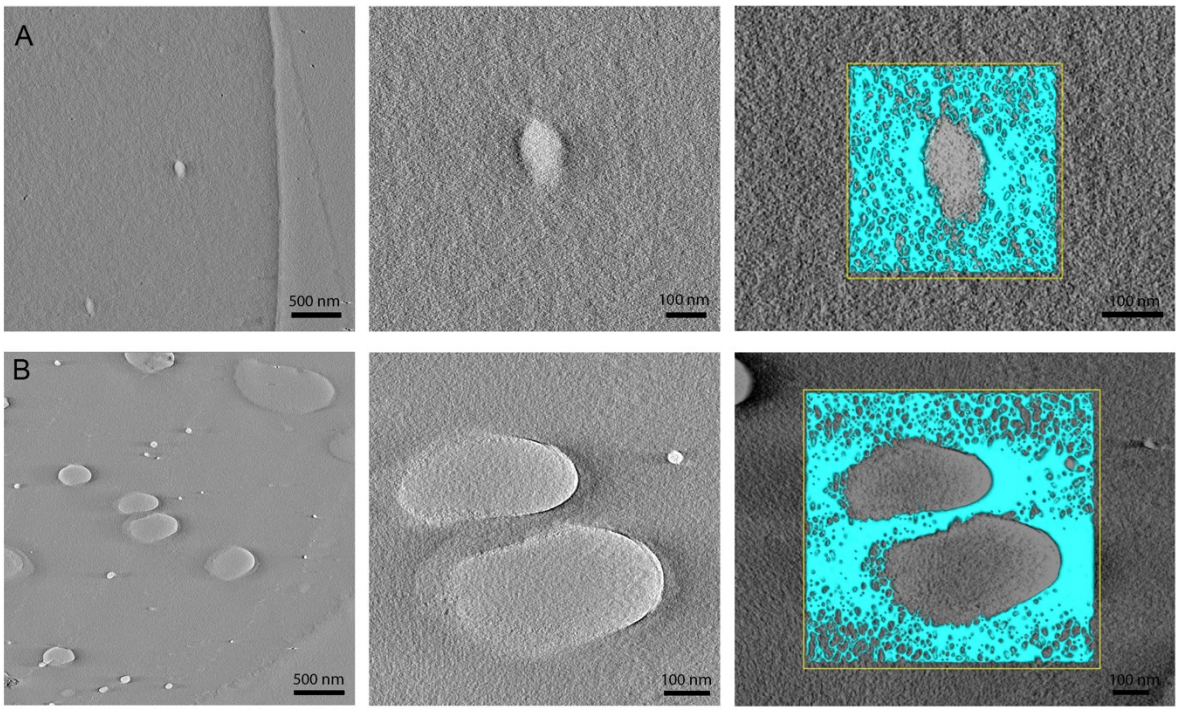

Fig. S3. A) TEM tomography of Mulberry (*B. mori*) silk displaying few small voids the features of which are more closely examined in panels 2 and 3. B) TEM tomography of Eri (*S. c. ricini*) silk displaying more numerous voids of varying sizes the features of which are more closely examined in panels 2 and 3. Note the relatively smooth inner surface of the voids in both the Mulberry and Eri silks, showing lack of any bridging nanofibrils.

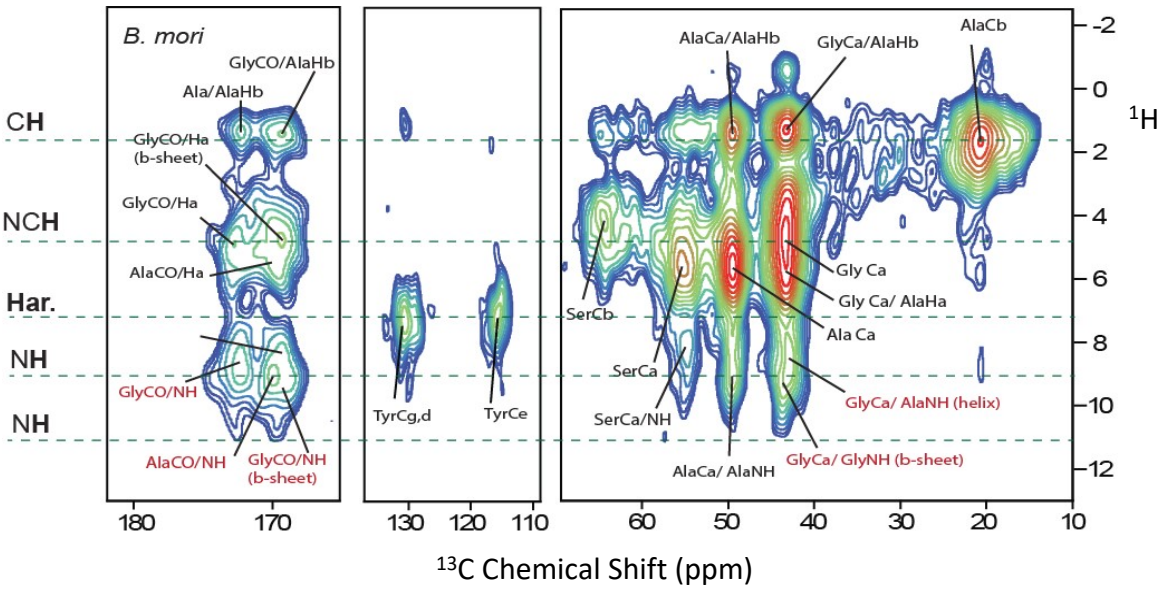

Fig. S4. Expanded ^{1}H-^{13}C HETCOR of Mulberry (*B. mori*) silk displaying the major peaks.

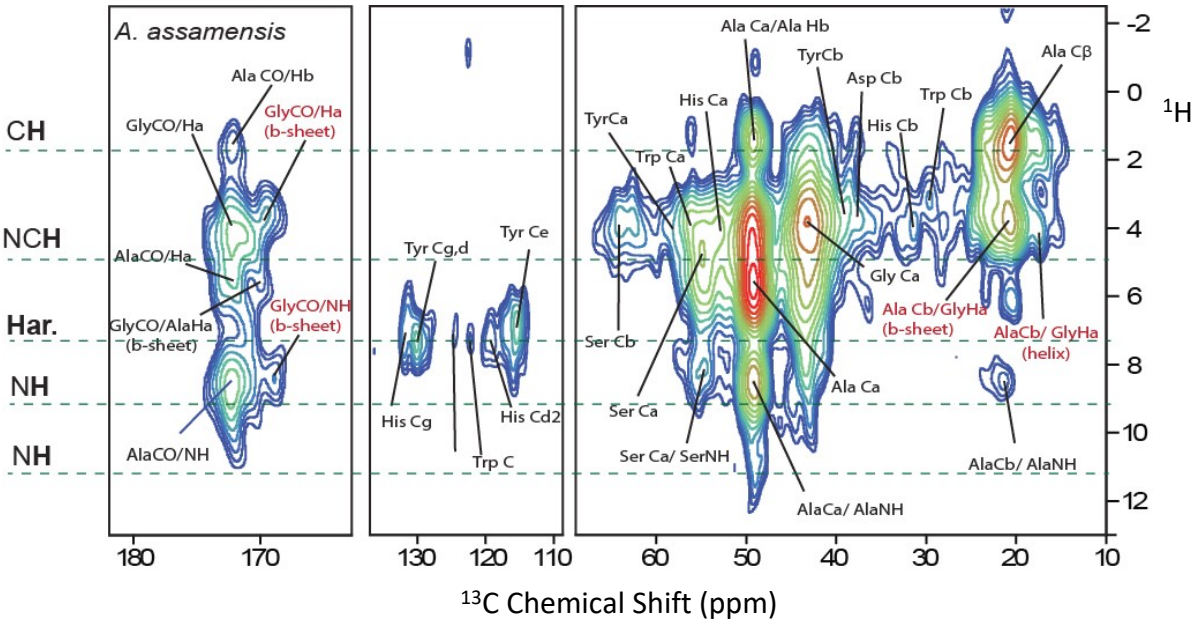

Fig. S5. Expanded ^{1}H-^{13}C HETCOR of Muga (*A. assamensis*) silk displaying the major peaks.

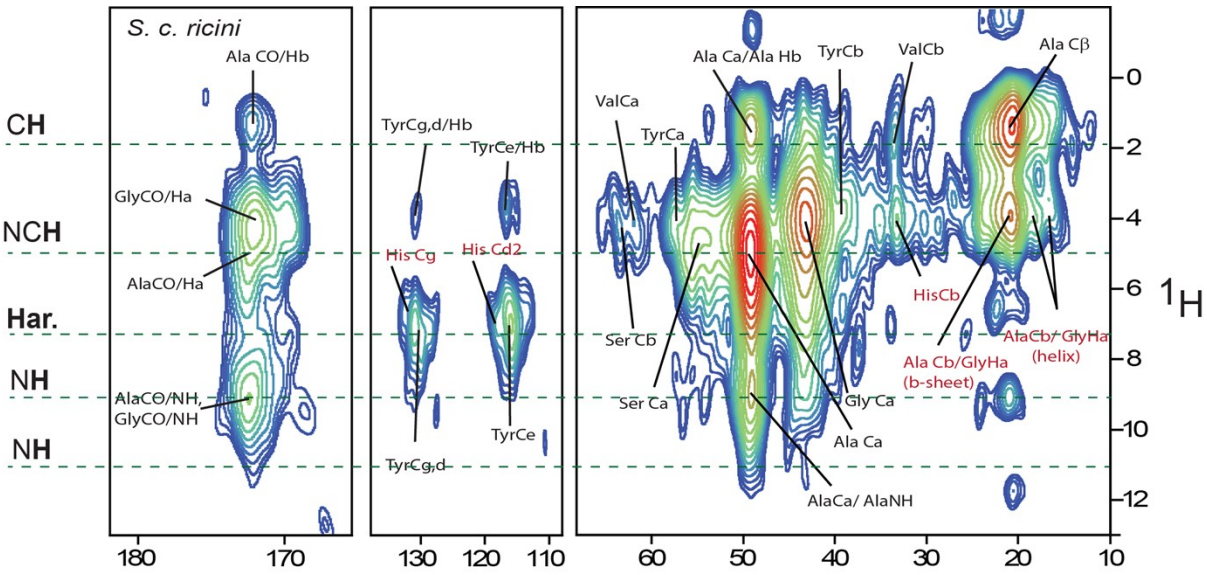

Fig. S6. Expanded ^{1}H-^{13}C HETCOR of Eri (*S. c. ricini*) silk displaying the major peaks.

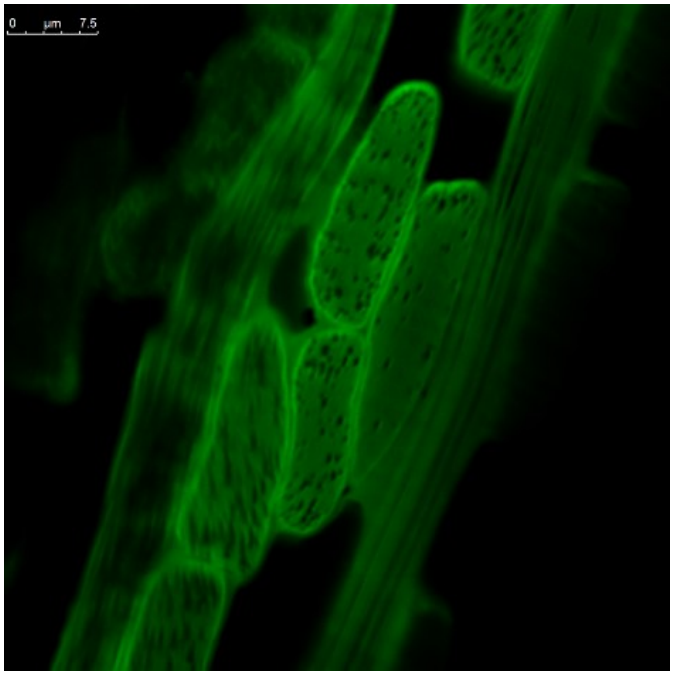

Fig. S7. Confocal microscopy image of cross section of a cocoon layer of muga silk prior to degumming, shows the presence of voids, just as was observed in the degummed fibres.

Comment [RR]: You may add this in the supplementary section and add

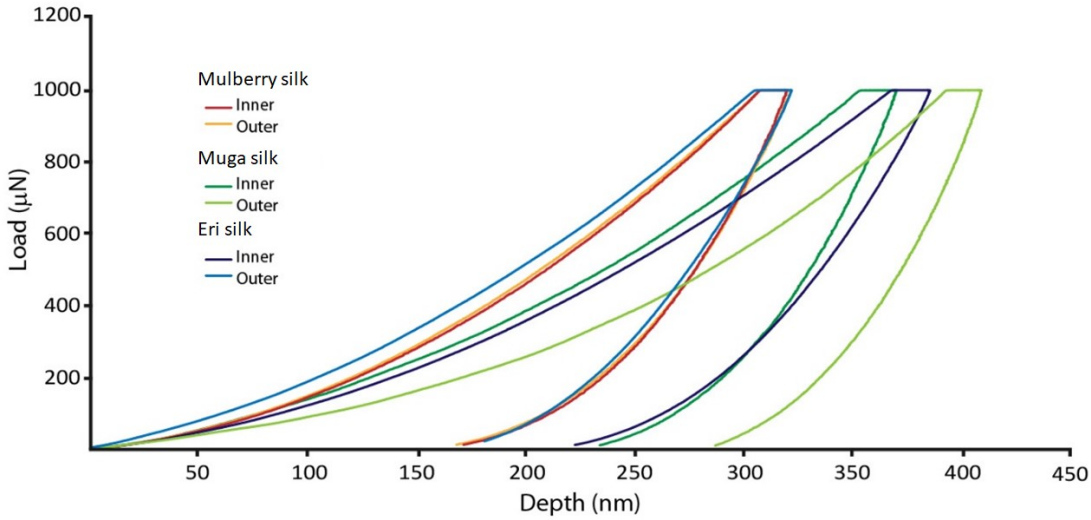

Fig. S8. Example load-depth curves for quasi static nano-indentation tests for determination of the reduced modulus Er.

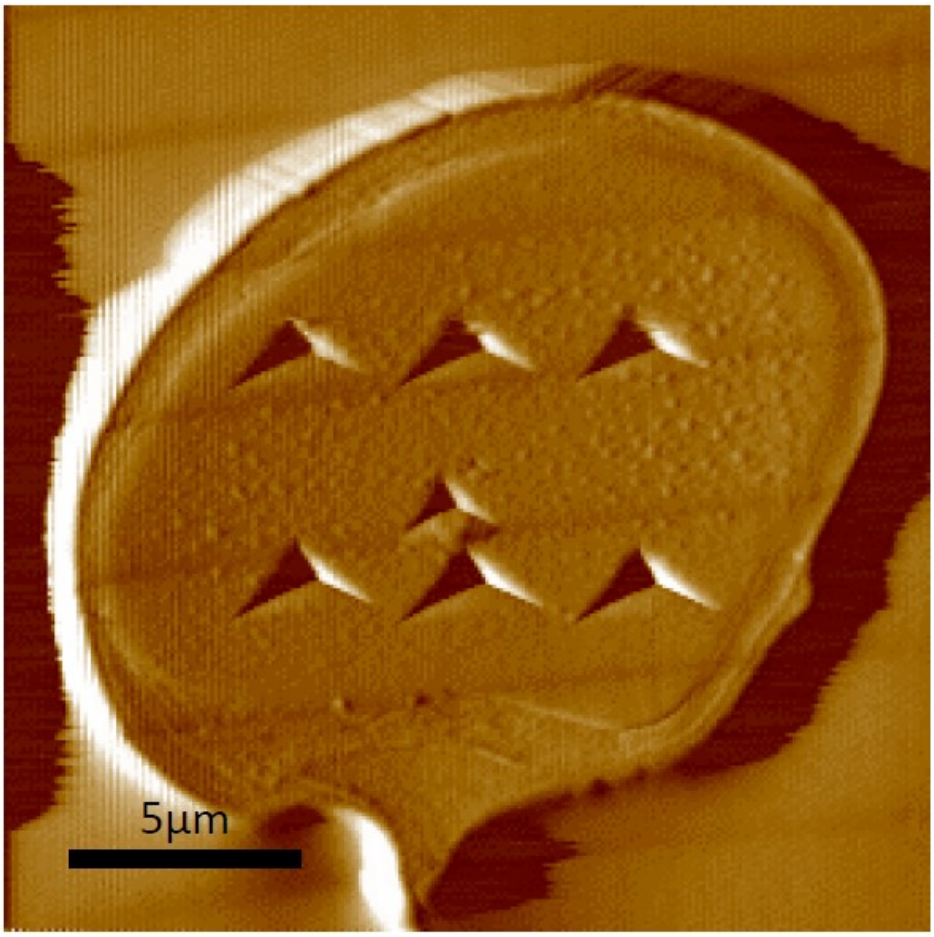

Fig. S9. Example AFM image of Mulberry (*B. mori*) silk displaying the nano-indentations that were analyzed for measuring the hardness.

Table S1a. Results (mean ± S.E. and results of MANOVA analyses of the means) of tensile testing of silk fibres taken from the inner and out portions of cocoons built by Muga (*A. assamensis*-Muga silk), Eri (*S. c. ricini*- Eri silk), and *Bombyx* (*B. mori*-Mulberry silk) silkmoths.

Tensile testing:			
Sample	Cross-sectional area $(\mu m)^2$ (n= 50)	Ultimate Stress MPa (n=50)	Strain % (n=50)
Eri_Inner	98.25 ± 43.18	464.12 ± 112.93	24.37 ± 7.52
Eri_Outer	126.37 ± 32.66	373.51 ± 76.74	28.30 ± 9.33
Muga_Inner	146.92± 18.26	765.04 ± 155.92	33.83± 11.13
Muga_Outer	164.26 ± 39.02	583.22 ± 129.05	32. 18± 11.50
Muberry_Inner	65.72 ± 23.33	605.59± 128.56	14.57 ± 4.31
Mulberry_Outer	80.73 ± 11.71	587.14± 119.52	16.19± 6.28
MANOVA:			
Wilk' lambda	0.877	0.845	0.983
F	31.991	43.817	27.713
P	<0.0001	<0.0001	<0.0001

On average in all the types of silk, the inner cross-sectional area of the silk fiber is smaller than that the outer cross-sectional area. Concomitantly, the inner sections of the fiber also yield higher ultimate stress values, with the Muga silk fiber showing the greatest difference, and the Mulberry silk showing the least difference in the tensile strength. The changes in the cross-sectional area and the tensile strength may represent the influence of changes in the mechanism of the silk spinning by the silkworm at different stages of the cocoon formation.

Table S1b. Results (mean ± S.E. and results of MANOVA analyses of the means) of nanoindentation in the axial and non-axial directions of silk fibres taken from the inner and out portions of cocoons built by Muga (*A. assamensis*), Eri (*S. c. ricini*), and *Bombyx* (*B. mori*) silkmoths. Er Axial = reduced modulus in the axial direction, H Axial = hardness in the axial direction, Er Non-Axial = reduced modulus in the non-axial direction, H Non-Axial = hardness in the non-axial direction.

Nanoindentation				
Sample	Er Axial (GPa) (n= 50)	H Axial (GPa) (n= 50)	Er Non-Axial (GPa) (n= 50)	H Non-Axial (GPa) (n= 50)
Eri_Inner	9.15 ± 2.10	0.43 ± 0.11	6.84 ± 1.69	0.40 ± 0.09
Eri_Outer	8.72 ± 3.19	0.46 ± 0.22	7.16 ± 2.54	0.48 ± 0.18
Muga_Inner	10.04 ± 2.66	0.43 ± 0.28	7.91 ± 2.01	0.39 ± 0.09
Muga_Outer	10.88 ± 3.67	0.40 ± 0.33	8.15 ± 3.09	0.42 ± 0.14
Mulberry_Inner	11.18 ± 1.35	0.48 ± 0.23	8.85 ± 1.08	0.48 ± 0.05
Mulberry_Outer	11.41 ± 3.03	0.52 ± 0.26	8.55 ± 2.28	0.50 ± 0.13
MANOVA:				
Wilk' lambda	0.004	0.002	0.009	0.003
F	0.959	0.711	2.092	0.566
P	0.339	0.450	0.104	0.512

Table S2. Relative percentage of β-sheet and helix/turn/random coil structures in the silk fibers determined from analysis of the Amide II peak in the FTIR (Figure S1).

	Inner		**Outer**	
Silk	β-sheet	helix/turn/random coil	β-sheet	helix/turn/random coil
Mulberry	50 %	50 %	49.8 %	50.2 %
Eri	48.6 %	51.4 %	47.9 %	52.1 %
Muga	41.3 %	58.7 %	40.9 %	59.1 %

Table S3. Example cross-sectional areas and void fractions for the different types of silk extracted from the inner and outer parts of the cocoon. Data extracted from AFM images using Image-J.

	Inner		**Outer**	
Silk	Area (μm^2)	Void fraction (%)	Area (μm^2)	Void fraction (%)
Mulberry	121.59	0.8	115.75	0.8
Eri	123.80	3.5	127.57	3.8
Muga	121.59	6.6	115.75	13.6